Study of the effect of bluff body size on stability limits of a premixed natural gas swirl burner

Milad Behzadi[1] · Seyed Hamzeh Siyadat[2] · Fathollah Ommi[1] · Zoheir Saboohi[3]

Abstract
Flame stabilization is highly important in lean premixed combustion which is considered a desirable technology for low-emission gas turbines. Swirl stabilization is one of the most common methods used for this purpose. Simple generation of swirl, however, is not enough to reach an acceptable operating range. A method of improving stability is using a bluff body in order to resist flame flashback caused by combustion-induced vortex breakdown at moderate to high swirl numbers. The present study aims to investigate the effect of bluff body size on the stability boundaries of flashback and blowout and also on flame shape. A premixed swirl burner is designed and built to operate with natural gas at atmospheric condition. In addition to gas and air flow rates at stability limits, normal and chemiluminescence flame images are documented. The non-reacting flow is also simulated to investigate the flow pattern out of the burner nozzle. It is found that bluff body size has a significant influence on flashback prevention and to a lesser extent on lean blowout limit while having minor effect on the shape of the flame. Just before blowout, low-frequency fluctuations are observed in the chemiluminescence radiations that are associated with the periodic changes in flame zone. Nonetheless, no warning signs are observed before flashback. Looking into the velocity profiles at the nozzle exit also shows an increase in axial velocity near the center of the nozzle with larger bluff bodies, revealing the mechanism of improvement of burner resistance to flame flashback.

Keywords Combustion · Flashback · Blowout · Chemiluminescence

List of symbols

c_b	Ratio of flow to flame velocity
d_1	Bluff body rod diameter (mm)
d_2	Bluff body head diameter (mm)
FA_s	Stoichiometric fuel-to-air ratio
g_1	Flashback correlation constant (W)
g_2, g_3	Flashback correlation constant
k	Turbulent kinetic energy ($m^2 s^2$)
$\dot{m}_a$	Air mass flow rate (kg s^{-1})
$\dot{m}_f$	Fuel mass flow rate (kg s^{-1})
p	Static pressure (Pa)
Q	Thermal power (W)
r_{cn}	Ratio of bluff body to nozzle diameter
Re	Reynolds number
S_L	Laminar flame speed (m s^{-1})
S_{L0}	Laminar flame speed at stoichiometry (m s^{-1})
SN	Swirl number
t	Time (s)
u_i	Velocity vector (m s^{-1})
U	Average axial nozzle velocity (m s^{-1})
x_i	Position vector (m)
α	Flame speed dependence on φ (m s^{-1})
β	Coefficient in dissipation equation
δ_{ij}	Kronecker function
E_{ij}	Mean strain rate tensor (s^{-1})
ε	Dissipation rate ($m^2 s^3$)
λ	Excess air ratio
μ	Kinematic viscosity (Pa s)
ρ	Density (kg m^3)
σ_d	Coefficient in dissipation equation
τ_{ij}	Specific Reynolds stress tensor ($m^{-2} s^{-2}$)
φ	Equivalence ratio
χ_ω	Dimensionless vortex stretching
ω	Specific dissipation rate (s^{-1})
Ω_{ij}	Mean rotation tensor (s^{-1})

✉ Fathollah Ommi
fommi@modares.ac.ir

1 Tarbiat Modares University, Tehran, Islamic Republic of Iran

2 K. N. Toosi University of Technology, Tehran, Islamic Republic of Iran

3 A&S Institute, Ministry of Science, Research, and Technology, Tehran, Islamic Republic of Iran

Introduction

Nowadays, lean premixed combustion is a desirable technology for gas turbines with its ability in reduction of pollutant emissions [1, 2]. Flame temperature of a premixed mixture of fuel and air with high excess air ratios is lower, resulting in minimum production of pollutants, especially nitrogen oxides [3, 4]. In this type of combustion, flame stabilization may partially be achieved by means of swirl. Stability range of a burner is first restricted by two phenomena: flame flashback and blowout. Flame flashback is caused by several reasons:

(1) Autoignition: Air and fuel are mixed before arriving at the flame and are at high temperature, facilitating autoignition [5].
(2) Thermo-acoustic instability: Catastrophic coupling of heat release and acoustic modes in a combustion chamber may lead to flame flashback [6].
(3) Flashback in boundary layer: With a low swirl intensity, flame can propagate through the boundary layer near the wall of the burner nozzle. A small increase in swirl intensity increases flow velocity near the wall and solve this problem [7, 8].
(4) Flashback in the core flow: Lower swirl intensities usually produce more pollutant emissions and designers tend to moderate and high swirl intensities. However, when swirl exceeds a critical value (depending on fuel type and flame conditions), the flame propagates upstream through the central region of the burner nozzle [9].
(5) Flashback due to combustion-induced vortex breakdown (CIVB): Flow velocity in the non-reacting flow may not be weak enough for the flame to propagate through, but the combustion can intensify the adverse pressure gradient and cause the recirculation zone to extend into the nozzle, leading to flashback [10, 11]. Flashback speed in this case is much greater compared to boundary layer mechanism [8].

Influence of coherent structures (i.e., vortex shedding and precessing vortex core) on flashback has been recently observed [12]. This possible mechanism is not clear enough yet and need to be studied more before it can be categorized separately.

Flame propagation during flashback has been the subject of several studies. It is known that the flame propagation involves turning around burner axis [13–15]. This rotation between the nozzle and the bluff body produces an adverse pressure gradient which in turn thickens the boundary layer around the bluff body and also escalates flow vorticity leading to a faster flashback [16, 17].

Some studies are oriented toward discovering the effect of flow and flame properties on flashback limits. Thermal power and burner flow rate influences its allowable equivalence ratio. At higher thermal powers, operating range extends [18]. Linear relation between excess air ratio at flashback and burner flow rate has been observed at certain conditions. Furthermore, flashback and blowout data have shown to collapse when tangential velocity plotted versus equivalence ratio [19]. A model has been presented for prediction of flashback [20] according to which flashback occurs when turbulence time scale in the recirculation zone exceeds reaction time scale. This model suits burners with lower Reynolds numbers, and for higher Reynolds numbers, simulating the recirculation zone with a well-stirred reactor gives better results [21].

The phenomena observed during flame blowout at low equivalence ratios had also been studied. Near blowout limit, swirl flames suffer from low-frequency, high-amplitude fluctuations manifested in the combustion chamber pressure [22]. A regularly V-shaped flame turns to an M-shaped one. In addition to the central recirculation zone, another recirculation zone evolves in the corner of the combustion chamber [23]. The presence of nanoparticles in the reactive mixture, whether impurities or purposely added, may affect stability limits since nanofluids have different velocity profiles and temperature boundary layer thicknesses [24] while passing over surfaces. Thermal radiation behavior is also affected by these particles [25]. Improving stability with the aid of magnetic field [26] is worth examining.

It has been found that a vortex breakdown would occur in the flow of a swirl burner, provided that the swirl intensity is sufficient [27]. As a result, without provisions, axial velocity becomes negative and flame flashback occurs. In practical swirl numbers, the last mechanism, CIVB, becomes important. Its occurrence depends on burner geometry in addition to flow rate, fuel type, and equivalence ratio [28]. A common remedy to overcome this problem is to inject an axial non-swirling stream through the center of the burner nozzle [11, 14, 29]. This method requires wise adjustment of mass flow ratio of axial to swirling flows. A method of burner design based on this technique has been presented [30]. Axial flow injection may cause susceptibility to boundary layer flashback. This problem can be solved by installation of a porous wall in the burner nozzle [31, 32]. Another way of overcoming CIVB is to place a bluff body in the center of the nozzle. Utilizing a bluff body in non-swirling flow is a way of flame stabilization by itself [33]. However, it is used here to fill the zone of weak or negative axial velocity. This method of overcoming flashback may be seen in the design of some research burners [12, 34, 35]. A burner without axial injection or bluff body is presented in Ref. [36], but its nozzle diameter is so small and this might be the reason of resisting flashback.

It is already known that the presence of a bluff body can help flashback resistance and is even vital in some deigns. This paper aims to discover how the size of bluff body affects this stability improvement and whether blowout limit is affected too. Furthermore, the effect of this geometry adjustment on flame and reaction zone is also investigated. The origination of this improvement is sought for in velocity profiles out of the burner nozzle. This paper is organized in five main titles. After this introduction, the methodology is explained in Sect. 2. Experimental setup and procedure and numerical analysis method is described in Sect. 3. The results are presented in Sect. 4 and discussed. Finally, concluding remarks are summarized in the last section.

Methodology

Using bluff body in swirl burners is not investigated in the literature so much. There exist few studies on bluff body role in flame stabilization for diffusion flames [37, 38] and partially premixed flames [12], but not for fully premixed flames. The theory of vortex bursting has been adapted for confined swirling flames with bluff bodies by Karimi [17], and the role of bluff body in centrifugal forces and adverse pressure gradient was theoretically revealed. It has also been observed that the flame propagation takes place around and adjacent to the central body [17]. As explained before, for applicable swirl numbers, i.e., SN = 0.6–1.0, a swirling flow alone would face flame flashback. The present burner is designed to yield such swirl numbers and preliminary experiments showed that without bluff body, no fuel-to-air ratio can build a stable flame.

The hypothesis is that the vortex structure produced by the swirl creates a low-velocity region in the center of the burner nozzle through which the flame propagates upstream. If this assumption is true, filling the low-velocity region with a, let's say, bluff body can solve the problem. The experimental and theoretical investigations by Karimi [17] showed that when the flame enters the nozzle annulus, the presence of a bluff body intensifies the adverse pressure gradient and causes the flame to faster propagate upstream. Thus, the bluff body size needs to be adjusted so that the flame is prevented from entering the annulus. Note that the purpose of using a bluff body is not producing divergence in the flow to form a recirculation zone behind the bluff body; this is achieved by the swirl itself. Naturally, the size of the filling body must be important since it is intended to take up a certain space. Changing the size of the bluff body is a minor modification, and it would be desirable to improve the stability of a burner via such a modification without modifying the swirler assembly, combustion chamber, or the nozzle diameter.

This hypothesis is first experimentally examined and approved. The reason of its viability is then investigated through numerical simulation. Stability limits of a laboratory burner with bluff bodies of different sizes are obtained at various thermal powers and compared. It would be beneficial to see how this modification affects the flame shape and the location of combustion reactions. Therefore, regular and chemiluminescence imaging is utilized to study the reaction zone. The nonreactive flow is then simulated including the whole burner components. Especially, attention is paid to the axial and tangential velocity components in the nozzle annulus. Although combustion affects the burner flow field, analysis of the velocity patterns that the nozzle delivers to the combustion chamber could elucidate the mechanism behind the difference that the bluff body size makes.

Experimental setup and numerical details

Experimental setup

The tests are conducted using an atmospheric confined burner. The experimental system shown in Fig. 1 was designed primarily for combustion instability studies and was adapted to current investigations. Air and natural gas enter a premixing tube which is 25 mm in diameter and 50 mm long as depicted in Fig. 2. This mixture then passes

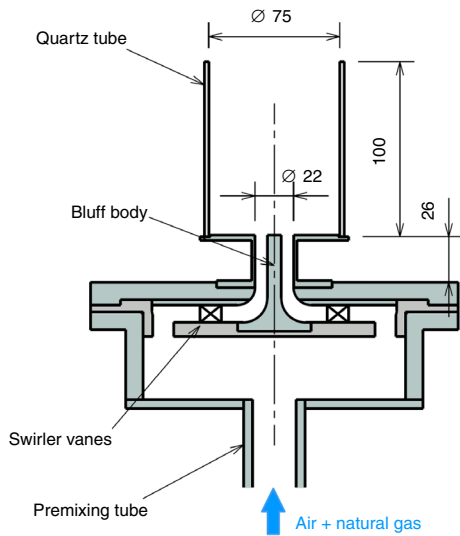**Fig. 1** Experimental setup including the burner and the instrumentations

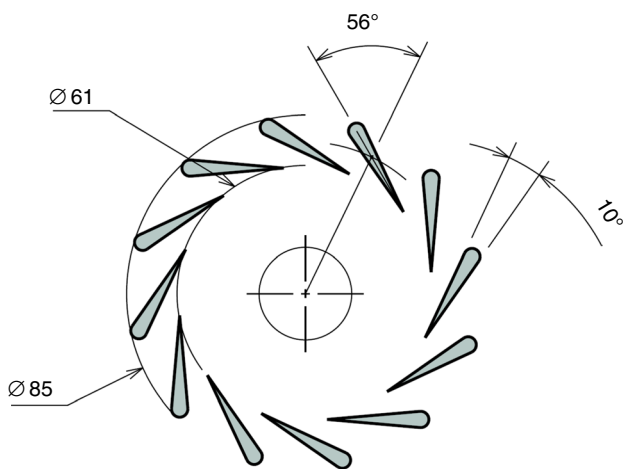**Fig. 2** Schematic of the burner and the path of gas flow inside (dimensions in millimeter)

Fig. 3 Top view of the swirler vanes (dimensions in millimeter)

Fig. 4 Cross section of the bluff bodies and their common dimensions (dimensions in millimeter)

Table 1 Distinctive dimensions of the bluff bodies and their identifiers

Bluff body ID	U8	$Y10$	$Y11$	$Y12$	$Y14$
Type	Cylindrical	Conical head			
d_1	8	6	7	8	8
d_2	8	10	11	12	14
r_{cn}	0.36	0.45	0.50	0.55	0.64

over the swirler vanes and enters the combustion chamber through the annular path between the nozzle tube and the bluff body. The swirler is of radial type with 12 equally spaced vanes. As depicted in Fig. 3, the vanes are installed at 56 degrees angle and each vane has 24 mm length and 10 mm height. The swirler design is adopted from a study by Sheen et al. [39] with few minor modifications for fabrication simplicity. This reference provides a relation for swirl number in terms of the vanes install angle. The combustion chamber is a quartz tube of 75 mm inner diameter and 100 mm length. The bluff body is interchangeable. Five different bluff bodies are tested in this burner whose drawi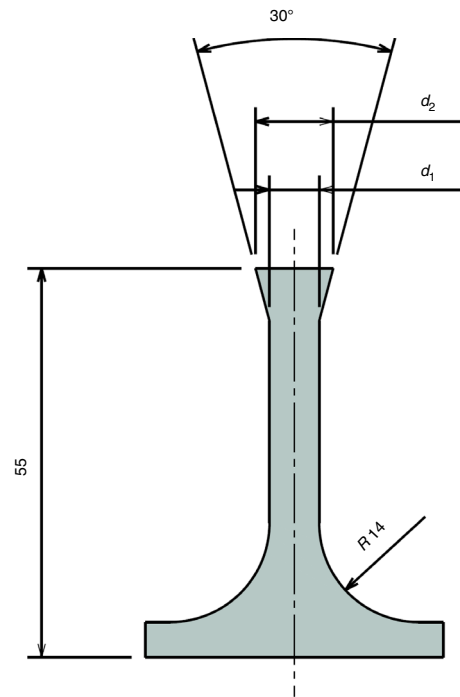ng is illustrated in Fig. 4, and their dimensions are listed in Table 1. All of them consist of a narrow cylinder and a cone in the upper part. With this design, it is expected that the flow area in the tube annulus would not become small and only the low-velocity region at the center of the nozzle will be filled with the cone. Furthermore, the divergence produced in the flow will improve the stability of the flame. The cylindrical bluff body is indicated with letter U, and those with a cone on their upper part are indicated with letter Y. The number following these letters indicates the upper diameter of the bluff body. The parameter r_{cn} is the ratio of this diameter to the nozzle diameter.

Air is supplied by a centrifugal blower whose speed (and thus the air flow rate) is adjusted via an inverter which alters the frequency of the electricity current. The air flow rate is measured with an Abzar Control Arshia

rotameter type flow meter with up to 10 m^3 h^{-1} measuring range and 0.2 m^3 h^{-1} maximum error. Natural gas is consumed as the burner fuel, and its flow rate is measured with Dwyer rotameter with up to 10 lit min^{-1} measuring range and 0.1 lit min^{-1} maximum error.

Although the composition of natural gas varies from region to region and even with time, its main constituent is methane (87–98%), the remainder being other hydrocarbons, nitrogen, and carbon dioxide. Chemical equilibrium calculations using CEA software considering different possible compositions, showed that the stoichiometric air-to-fuel ratio is a little lower than that of pure methane, typically 15.7 as compared to 17.1 of methane. Adiabatic flame temperature of these mixtures is very close to that of pure methane, 2220 K under stoichiometric conditions, and reduces to 1480 with 100% of excess air. These calculations also show that the main constituents of the combustion products are the same for different fuel-to-air ratios, except the small amount of CO under near stoichiometric conditions disappears at higher excess air ratios.

Two types of flame imaging are carried out. Normal flame images are taken with a Nikon P510 camera, and chemiluminescence images are recorded with a Canon EOS 750D camera. In front of the later, a Thorlabs FB430-10 bandwidth filter is placed with center wavelength of 430 nm and 10 nm width. This wavelength is generated by CH* radicals. Flame chemiluminescence intensity is measured with a Thorlabs PMM01 photomultiplier, and an ASAHI Spectra XBPA310 UV optical filter with center wavelength of 310 nm and width of 10 nm. This wavelength is related to OH* radicals. It has been demonstrated that the intensity of the CH* and OH* chemiluminescence is proportional to the instantaneous flame heat release [40, 41]. The error of the photomultiplier for current conditions is 0.3%.

The velocity of the flow exiting from the premixing tube is measured with a hot film sensor (calibration process in [42]) before entering the swirler to look for possible fluctuations. RMS of velocity fluctuations is only 2% indicating that the flow supplied by the blower and delivered to the burner assembly is quite uniform.

Experimental procedure

The bluff bodies are examined with different available thermal powers and excess air ratios. These conditions cover Reynolds numbers of 640–5300 and thermal powers of 0.95–5.7 kW. Reynolds number is defined based on nozzle average velocity and hydraulic diameter. For each of the bluff bodies, the gas flow rate is set to a specific value and the air flow rate is then set to a value that resulted in an excess air ratio suitable for flame ignition. Igniting the burner is easy in the presence of the flame tube provided that the excess air ratio is not near the blowout limit. All the results presented in this paper are related to tests carried using the flame tube. However, we noticed that without this flame tube, it would not be that easy to ignite the flame. Having ignited the flame, the gas flow is kept constant and the airflow is raised gently until blowout occurred. Once again, after turning on the flame at the same gas flow rate, the airflow is lowered until the flame encountered flashback. Alternation of the air flow is done slowly to achieve quasi-steady conditions and avoid any unwanted transient effect. The abovementioned procedure is repeated two or three times for a certain fuel flow rate and the same results are observed each time. Additionally, for flame shape analysis, certain operating conditions are set including three levels of thermal power and four excess air ratios from near stoichiometry to lean. These operating conditions are listed in Table 2.

When part or whole of the flame enters the nozzle, flashback is considered to occur, whether this caused the mixture inside the burner to explode or the flame merely settled inside the nozzle. On the other hand, extinction of the flame due to high air flow is regarded as blowout.

Numerical approach

The steady non-reacting flow is simulated to identify the flow pattern out of the burner nozzle. Since Mach numbers in this investigation are very low and there is no substantial pressure change, we have the opportunity to consider the flow as incompressible. Due to the axial periodicity, one-twelfth of the geometry is simulated and periodic boundary conditions are applied to the lateral surfaces. The simulation domain includes the swirler assembly but not the premixing tube. A section of the domain is shown in Fig. 5. Mass flow is set on the inlet which is the annulus beneath the swirler assembly. Environmental pressure is set on the outlet of the combustion chamber. In order to validate the numerical method, the cold flow of the burner presented in [39] which is very similar to the current burner is solved and the results are compared to the experimental data.

Reynolds stress method (RSM) is applied with stress-omega model for turbulence modeling. The governing equations of this steady incompressible flow are adapted from Wilcox [43]. The continuity

Table 2 Burner operating conditions for flame imaging and shape analysis

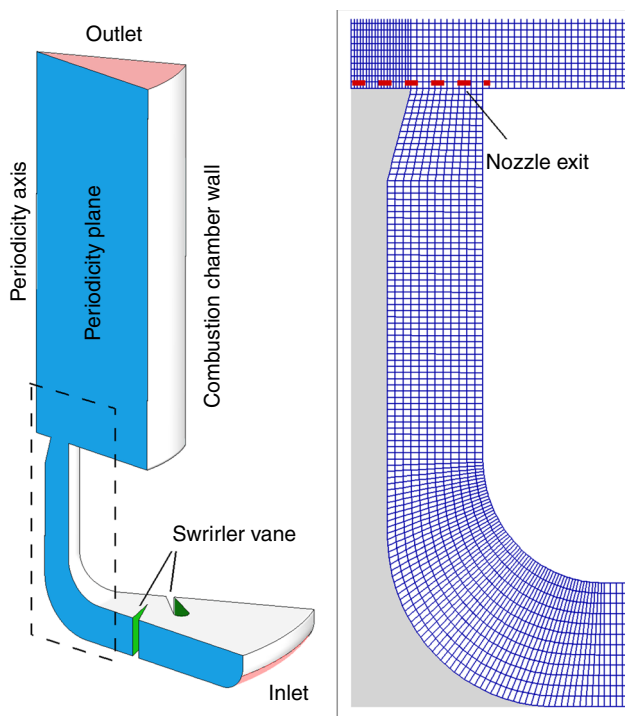| Parameter	Values			
Thermal power/kW	1.9	3.2	4.4	
Excess air ratio/%	5	18	35	58

Fig. 5 Computational domain volume and a detail view of the mesh

$$\frac{\partial \bar{u}_i}{\partial x_i} = 0 \tag{1}$$

and the momentum conservation equations

$$\rho \bar{u}_j \frac{\partial \bar{u}_i}{\partial x_i} = -\frac{\partial \bar{p}}{\partial x_i} + \frac{\partial}{\partial x_j}\left(2\mu E_{ij} + \rho \tau_{ij}\right) \tag{2}$$

are solved. Here u, p, ρ, μ are velocity, pressure, density, and dynamic viscosity, respectively. The prime sign denotes fluctuating parts, and the bar sign indicates mean flow parameters. The tensors E_{ij} and τ_{ij} are the mean strain rate and specific Reynolds stress tensors, respectively, defined by

$$E_{ij} = \frac{1}{2}\left(\frac{\partial \overline{u_i}}{\partial x_j} + \frac{\partial \overline{u_j}}{\partial x_i}\right), \quad \tau_{ij} = -\overline{u_i' u_j'}. \tag{3}$$

The specific Reynolds stress tensor should be tackled via Reynolds stress transport equation:

$$\frac{\partial \tau_{ij}}{\partial t} + \overline{u_k}\frac{\partial \tau_{ij}}{\partial x_k} = -\tau_{ik}\frac{\partial \overline{u_j}}{\partial x_k} - \tau_{jk}\frac{\partial \overline{u_i}}{\partial x_k}$$
$$+ \frac{\partial}{\partial x_k}\left[\frac{\mu}{\rho}\frac{\partial \tau_{ij}}{\partial x_k} + \overline{u_i' u_j' u_k'} + \overline{\frac{p'}{\rho}\left(\delta_{kj}u_i' + \delta_{ik}u_j'\right)}\right] \tag{4}$$
$$- \overline{\frac{p'}{\rho}\left(\frac{\partial u_i'}{\partial x_j} + \frac{\partial u_j'}{\partial x_i}\right)} + 2\frac{\mu}{\rho}\overline{\frac{\partial u_i'}{\partial x_k}\frac{\partial u_j'}{\partial x_k}}$$

where δ_{ij} is Kronecker delta function. The last term on the right side is the dissipation rate ε which is related to turbulent kinetic energy k and specific dissipation rate ω through

$$\varepsilon = 0.09 \, k \, \omega. \tag{5}$$

The equation solved for ω is

$$\frac{\partial \omega}{\partial t} + \bar{u}_j \frac{\partial \omega}{\partial x_j} = \frac{13}{25}\frac{\omega}{k}\tau_{ij}\frac{\partial \bar{u}_i}{\partial x_j} - \beta\omega^2$$
$$+ \frac{\sigma}{\omega}\frac{\partial k}{\partial x_j}\frac{\partial \omega}{\partial x_j} + \frac{\partial}{\partial x_j}\left(\left(\frac{\mu}{\rho} + \frac{1}{2}\frac{k}{\omega}\right)\frac{\partial \omega}{\partial x_j}\right) \tag{6}$$

while k is calculated based on the three normal Reynolds stresses by

$$k = \frac{1}{2}\overline{u_i' u_i'}. \tag{7}$$

The complementary relations and coefficients as suggested by Wilcox are

$$\beta = (0.0708)\frac{1 + 85\chi_\omega}{1 + 100\chi_\omega}$$
$$\sigma = \begin{cases} 0, & \frac{\partial k}{\partial x_j}\frac{\partial \omega}{\partial x_j} \leq 0 \\ \frac{1}{8}, & \frac{\partial k}{\partial x_j}\frac{\partial \omega}{\partial x_j} > 0 \end{cases} \tag{8}$$

where the dimensionless vortex stretching parameter χ_ω is defined by

$$\chi_\omega \equiv \left|\frac{\Omega_{ij}\Omega_{jk}E_{rmi}}{(0.09\,\omega)^3}\right| \tag{9}$$

and the mean rotation tensor Ω_{ij} is defined by

$$\Omega_{ij} = \frac{1}{2}\left(\frac{\partial \overline{u_i}}{\partial x_j} - \frac{\partial \overline{u_j}}{\partial x_i}\right). \tag{10}$$

The fourth term on the right side of Eq. (4) is called pressure strain and is handled based on ω equation through an approach presented by Launder–Reece–Rodi (LRR) [44]. To solve the abovementioned equations, ANSYS FLUENT 19.1 commercial software is used. Spatial discretization is second-order implicit, and SIMPLE method is used for pressure–velocity coupling.

Results and discussion

Experimental results

The burner can work for hours without any change in flame appearance or behavior. The only part of the burner that

heats up is the bluff body. However, this heating is not so great as to change its shape or size. The diameter of bluff bodies head does not change even after hours of burner work. In this section, first, the flame images, the effect of working conditions, and the size of bluff body on the flame shape are presented. In addition to the effect of bluff body size (which is the main subject of this study) on the flame, the effect of working conditions is also significant so that it cannot be ignored. Then, the effect of bluff body size on flashback and blowout limits is discussed.

Figures 6–8 show the normal flame images of $Y10$, $Y12$, and $Y14$ configurations, respectively, for different thermal powers and excess air ratios leading to stable flames. These conditions are marked in thermal power and excess air plane of Figs. 11 and 12. Despite the $Y12$ and $Y14$ configurations, the set of the images is not complete for the $Y10$ configuration since for some excess air ratios and thermal powers no stable flame can be obtained.

Two recirculation zones are observed in the combustion chamber. One is a central recirculation zone seen in all working states and the other a corner recirculation zone formed in some situations. The later forms in a toroidal shape near the interface between the wall and the floor of
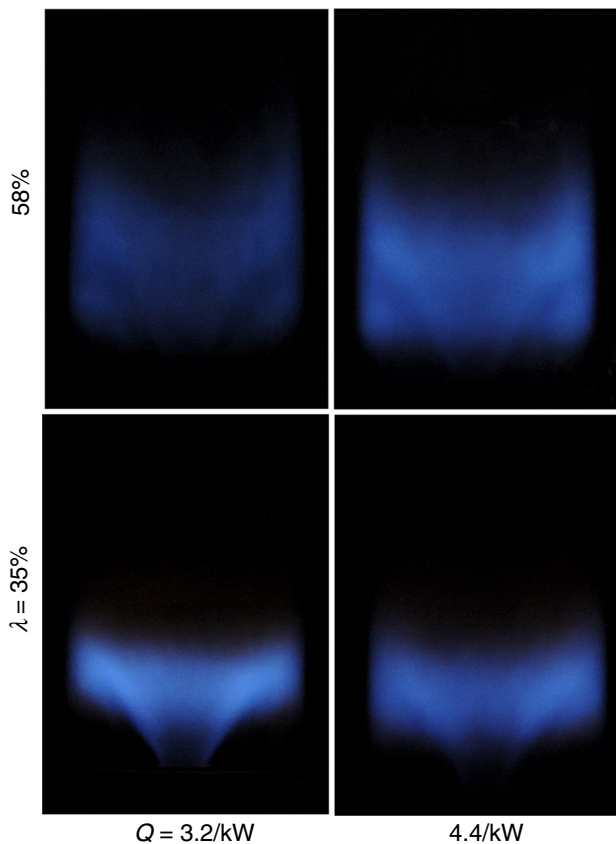

Fig. 7 Normal flame images of $Y12$ configuration at different thermal powers and excess air ratios

Fig. 6 Normal flame images of $Y10$ configuration at different thermal powers and excess air ratios leading to stable conditions

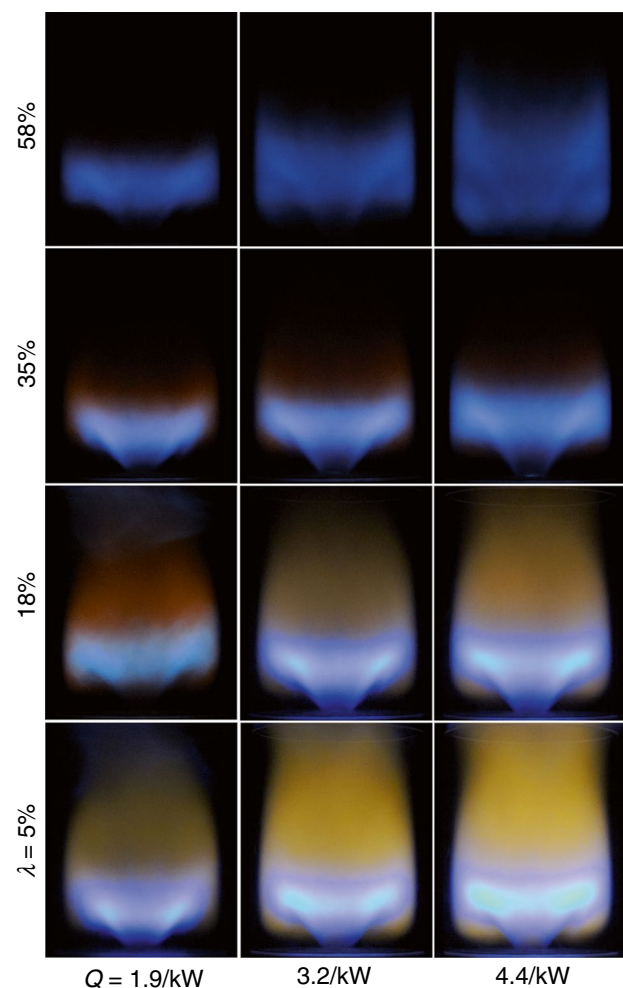the flame tube. When flow rate is high and equivalence ratio is low, the flow time scale is small and the reaction time scale grows, rendering a small Damkohler number. As a result, the flame cone must extend while it is limited by the chamber. The reacting flow bifurcates upon impingement on the wall. One branch climbs up and forms a flame shell on the tube wall and the other goes down and soon touches the floor and creates the corner recirculation zone. The effect of equivalence ratio is more significant at high thermal powers since higher flow velocity assists the effect of lower flame speed. Altering the equivalence ratio affects flame luminescence too. The violet-blue color at high excess air is due to the light emitted by CH* excited radicals decaying to lower energy levels [45]. Decreasing the excess air causes the emergence of C_2^* chemiluminescence with a green color and makes the flame appear sky blue. At near stoichiometry, CO_2^* broadband chemiluminescence along with black body radiation of probable hot tiny particles adds the yellow emissions [46].
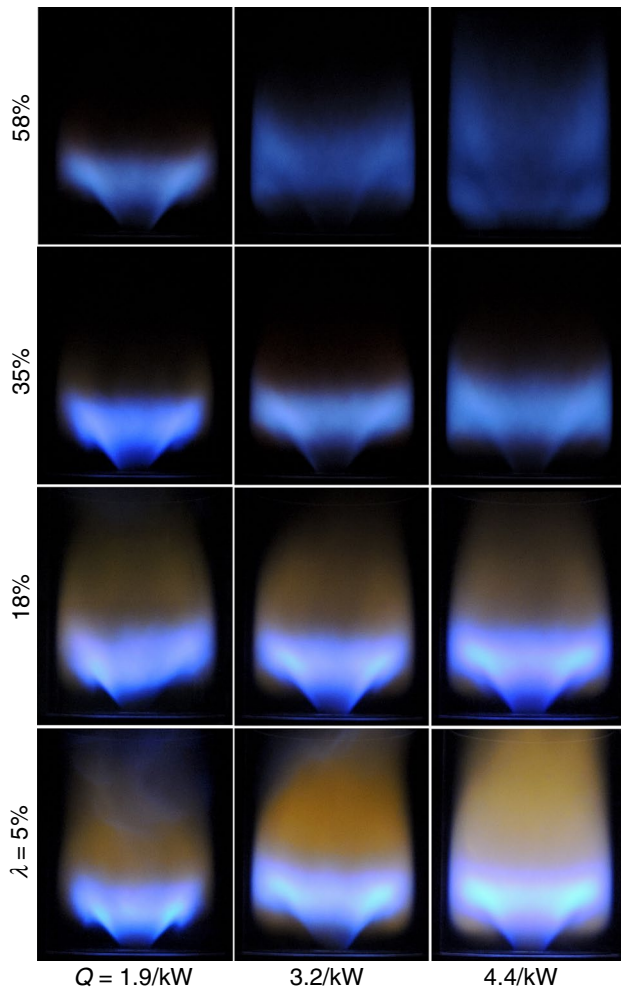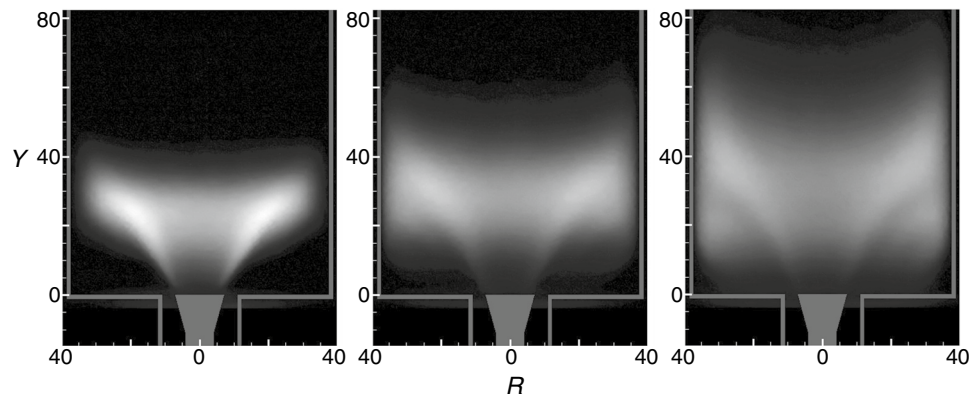
Fig. 8 Normal flame images of *Y*14 configuration at different thermal powers and excess air ratios

Thermal power has a noticeable effect on the flame shape. Figure 9 shows the CH* chemiluminescence for *Y*14 configuration and excess air ratio of 58%. These three images belong to three thermal powers of 1.9, 3.2, and 4.4 kW. As the thermal power increases, the flame cone

length must increase while the chamber dimensions are constant. Therefore, a greater volume of the tube is occupied by the reaction zones.

The flame shapes of bluff bodies *Y*10 and *Y*14 (with the biggest diameter difference) are compared. Flames of these configurations for excess air ratios of 35 and 58 percent are shown in Fig. 10. Abel deconvolution [47] is performed on the chemiluminescence images to show heat release trace in the diametric plane of the flame. For low excess air ratio, there is no significant difference between flame shapes of the two configurations, except flame height is slightly shorter and flame brush slightly thicker for the *Y*14 configuration. On the other hand, differences are more apparent for the higher excess air ratio. Both flames reach the wall; however for the thicker bluff body, a larger part of the flame brush deviates from the burner axis and approaches the wall while for the smaller bluff body, the flame maintains its conical shape.

Flashback and blowout limits are studied for different bluff bodies. Two types of flashback are observed. It happened whether explosively, that is, the flame entered the nozzle and the swirler assembly and burned the mixture in a flash or entered the nozzle and settled around the bluff body in a cylindrical shape. In the latter form, the bluff body becomes too hot and the flame begins to growl. With the U8 bluff body, if the excess air ratio is low enough to ignite the mixture, flashback will immediately happen and no flashback limit could be recognized for it. On the contrary with the Y bluff bodies, the flame never located inside the nozzle under stable conditions, but it is wholly over the head of the bluff body and outside the nozzle.

Figure 11 shows how bluff body diameter affects flashback limit, where excess air ratio at flashback is plotted versus thermal power. The region above each curve pertains to stable operation while no flame may exist in the region below the curves. The symbols are direct experimental data, and the curves fitted to them are functions that are derived based on Konle's model [20] through a process described here. According to Konle's model, for a certain burner
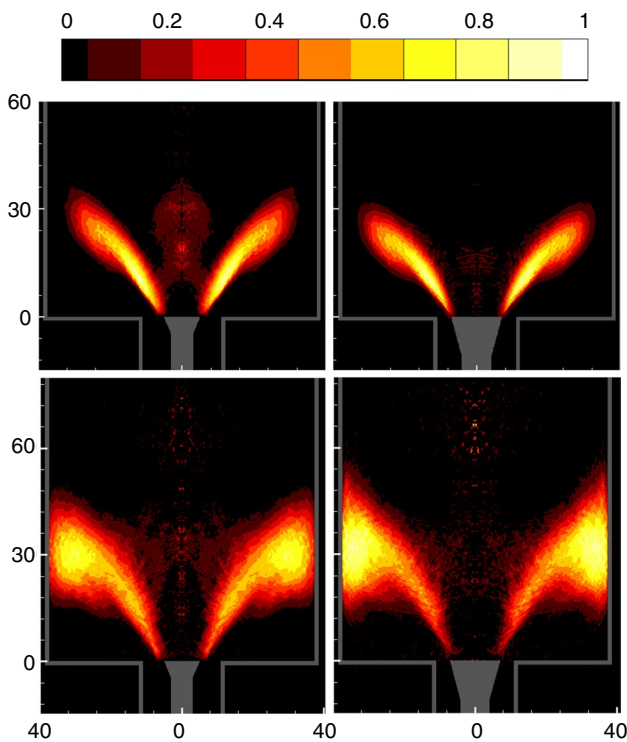
Fig. 9 Flame chemiluminescence for *Y*14 and excess air ratio of 58% for three thermal powers of 1.9, 3.2, and 4.4 kW from left to right
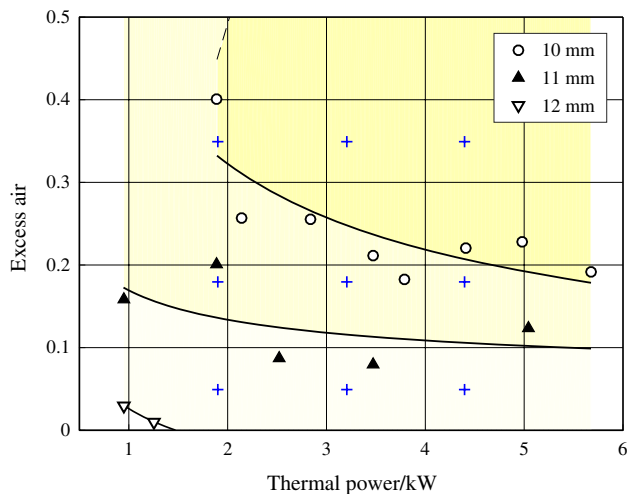
$$\frac{U}{S_\mathrm{L}} = c_\mathrm{b} \tag{11}$$

Average flow velocity, the nominator, is proportional to the air and fuel mass flow rate.

$$U \propto \dot{m}_\mathrm{a} + \dot{m}_\mathrm{f} \tag{12}$$

Based on the definition of equivalence ratio φ, and thermal power proportionality to fuel mass flow rate, it may be written as

$$U \propto Q\left(1 + \frac{1}{\varphi \cdot \mathrm{FA_s}}\right) \tag{13}$$

where $\mathrm{FA_s}$ is stoichiometric fuel-to-air ratio. For the range of equivalence ratios equal to or smaller than unity, it may be assumed that the laminar flame speed is linearly related to equivalence ratio [48].

$$S_\mathrm{L} = S_\mathrm{L0} + \alpha\,\varphi \tag{14}$$

According to Eq. (11), the ratio of the right-hand side of Eqs. (13) and (14) must be a constant. Thus

$$Q \propto \frac{S_\mathrm{L0} + \alpha\,\varphi}{1 + \left(\varphi \cdot \mathrm{FA_s}\right)^{-1}} \tag{15}$$

Substituting equivalence ratio with excess air ratio λ gives the following equation for the relation of excess air ratio and thermal power at flashback

$$Q = g_1 \frac{g_2 + (1 + \lambda)^{-1}}{g_3 + \lambda} \tag{16}$$

where g_is are constants. The derived relation represents the experimental data fairly well. It is worth noting that the assumption behind this model is that flame speed in the bottom of the recirculation bubble is approximately equal to laminar flame speed. Therefore, it may be concluded that for the mass flow rates studied here, the assumption of low flow turbulence in the nose of the recirculation bubble is valid.

The important finding is that a change in the size of bluff body can move the flashback limit. Using the $Y10$, $Y11$, and $Y12$ bluff bodies causes the flashback limit to recede step by step. With the $Y10$ bluff body, the blowout limit reaches the flashback limit at 1.8 kW. Thus, no stable flame exists for lower thermal powers. In other words, the burner suffers from either blowout or flashback at low thermal powers. This is the case for the U8 bluff body for the whole range of thermal powers where no stable flame can be obtained at any excess air ratio. Increasing the size of the bluff body from $Y10$ to $Y11$ makes it possible for the burner to operate with lower excess air ratios. Going to $Y12$ configuration helps the burner to be resistant against flashback except for very low thermal powers. The burner is stable for higher thermal

Fig. 10 Flame CH* chemiluminescence after Abel transform for thermal power of 3.2 kW, excess air ratios of 35% (up) and 58% (down), $Y14$ (right) and $Y10$ (left) configurations

Fig. 11 Flashback limits at various thermal powers for different bluff body sizes. Plus signs show conditions of images, blowout limits shown by dash lines

geometry, the ratio of average flow velocity out of the nozzle U at flashback, to laminar flame speed S_L, is constant, i.e.,

powers at any excess air ratio. The corresponding curve terminates by reaching $\lambda = 0$, because stoichiometry is the worst condition, and if a flame resists to flashback at stoichiometry, it will be stable at rich conditions too. Furthermore, as stated in Introduction, since low amount of pollutant emissions is achieved with lean combustion, this study concentrates on lean combustion and the figure includes lean ($\lambda > 0$) and stoichiometric ($\lambda = 0$) flames. With $Y14$ configuration, the problem of flame flashback wholly vanishes. Therefore, using a bluff body with 0.64 diameter ratio solves the problem of flashback for the range of thermal powers studied here.

The effect of bluff body size on blowout limit is another subject of study. Excess air ratio at lean blowout is plotted versus thermal power in Fig. 12. The region below each curve pertains to stable operation while no flame may exist in the region above the curves. At higher thermal powers, blowout limits of all configurations approach the same value: 75% excess air ratio. This indicates that at higher Reynolds numbers, blowout limit is independent of bluff body size. Note that increasing thermal power while keeping the excess air ratio implies that mass flow rate and Reynolds number are increasing. The recirculation zones are produced by both the bluff body and the swirl. It had been found that as Reynolds increases, the jet exiting from the nozzle stretches outward and divergence of the flow and the recirculation intensifies [49]. Thus, the contribution of the swirl in production of recirculation prevails and the size of bluff body has negligible effect on the recirculation zone. As can be seen from the upper row of the flame images, the flame cone extends at higher Reynolds numbers with high excess air ratios so that the recirculation zones are more defined by the confinement which is the same for all configurations.
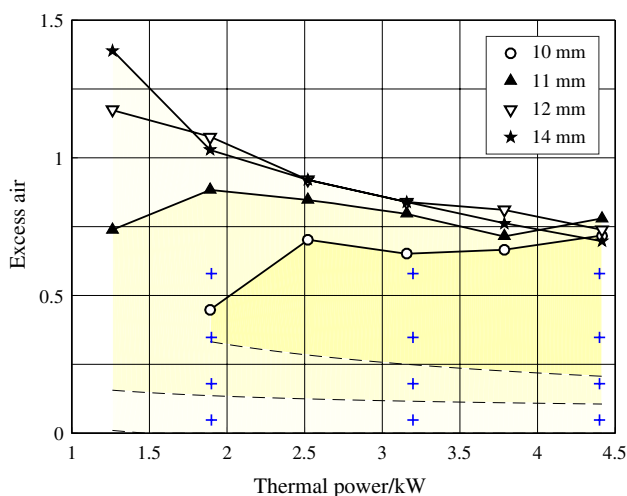
There is no data point beyond 4.4 kW since it is not possible to provide adequate air flow to obtain blowout. On the other hand, at lower thermal powers, blowout limit is affected by bluff body size and the positive effect of increasing the bluff body size can be seen. With $Y10$ configuration, flashback and blowout limits coincide and no stable flame could be reached at 1.8 kW and also for lower thermal powers. It is interesting to see that blowout limits of $Y12$ and $Y14$ configurations are the same. Thus, increasing bluff body size over diameter ratio of 0.55 is not necessary from the viewpoint of flame blowout.

Before blowout, low-frequency, high-amplitude oscillations appear in the flame. The corner recirculation zone extinguishes and then ignites again periodically and the location of this recirculation zone changes as well. OH* chemiluminescence of the flame for the $Y10$ configuration at 3.2 kW is shown in Fig. 13 when the excess air ratio is gently increased by increasing air flow rate until blowout happens. This phenomenon should not be mistaken with thermo-acoustic instability, as those large-amplitude flame dynamics have different signal footprints [50]. For other configurations and thermal powers, the behavior is the same and there is no need to repeat those graphs. The gradual fall of the mean value is due to decrement of equivalence ratio which weakens the chemiluminescence intensity. As the conditions tend toward blowout, the low-frequency oscillations in heat release rate grow. The frequency of these oscillations is approximately 6 Hz. Similar fluctuations are observed in pressure near blowout in studies reported in Ref. [23]. Such fluctuations may be considered a warning sign of flame blowout.

In spite of blowout, flashback occurs without any alert. Figure 14 shows OH* chemiluminescence history of the flame at 3.2 kW for $Y10$ configuration while approaching flashback by reduction of air flow rate. The mean intensity grows due to increment of equivalence ratio (as observed in [51]). Chemiluminescence intensity suddenly drops once flashback occurs. The reason in this case is that part of the flame settled in the nozzle and swirler assembly and went out of the photomultiplier sight. In case of explosive flashback,
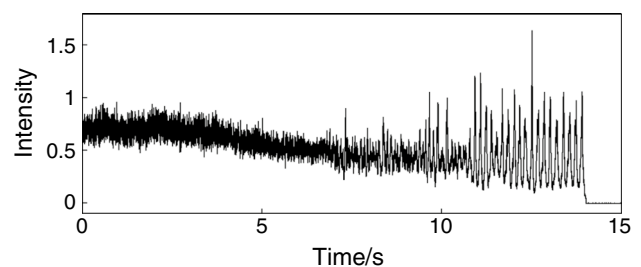

Fig. 12 Blowout limits at various thermal powers for different bluff body sizes. Plus signs show conditions of images, flashback limits shown by dash lines

Fig. 13 OH* chemiluminescence history of the flame on the approach to blowout for $Y10$ bluff body at 3.2 kW
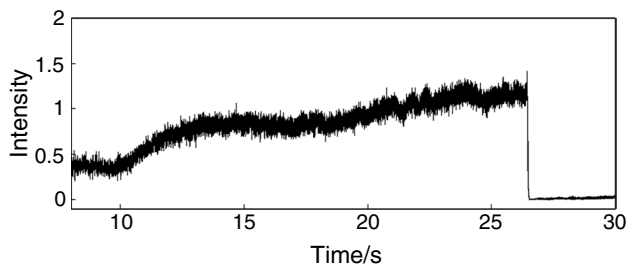
Fig. 14 OH* chemiluminescence history of the flame on the approach to flashback for $Y10$ bluff body at 3.2 kW

the intensity falls to absolute zero. For other configurations and thermal powers, the trends are the same. More sophisticated techniques as presented in [52] may be able to detect signs of flashback in the chemiluminescence signal.

Cold flow numerical results

Now that it is demonstrated that adjusting the diameter of bluff body can improve the stability range, especially its resistance to flashback; it would be appealing to seek for an explanation for the cause of this effectiveness. Flame propagation into the nozzle takes place when the flame speed prevails over flow velocity. Therefore, one must look for the cause in the velocity pattern of the burner nozzle exit. Two bluff bodies with the greatest diameter difference, $Y10$ and $Y14$, are analyzed in order to make the effect of the bluff body size more apparent. These two are similar in shape, but $Y10$ configuration failed to provide a stable flame under some conditions.

Velocity profiles at the exit of the nozzle and entrance of the flame tube which play a major role in flame stability are examined. Figure 15 shows the axial velocity, and Fig. 16 shows the tangential velocity for the abovementioned configurations for different Reynolds numbers corresponding to the flow rates tested. The axial velocity increases with radius in both cases and the maximum velocity occurs approximately near the wall of the nozzle. In $Y10$ configuration, the axial velocity drops substantially near the center, so that it reaches approximately zero near the bluff body. In $Y14$ configuration, the axial velocity undergoes smaller changes so that even for the smallest Reynolds number it has a significant value near the bluff body. The behavior of tangential velocity is somehow similar to the axial velocity. Here, the maximum velocity occurs slightly away from the wall of the nozzle. These velocity profiles are similar to those of the burners with radial swirler, with short nozzles after the swirler [53].

Velocity contour and path lines are shown at a similar flow rate of 8.5 m³ h⁻¹ for these two configurations in Figs. 17 and 18. Although the velocity patterns are generally
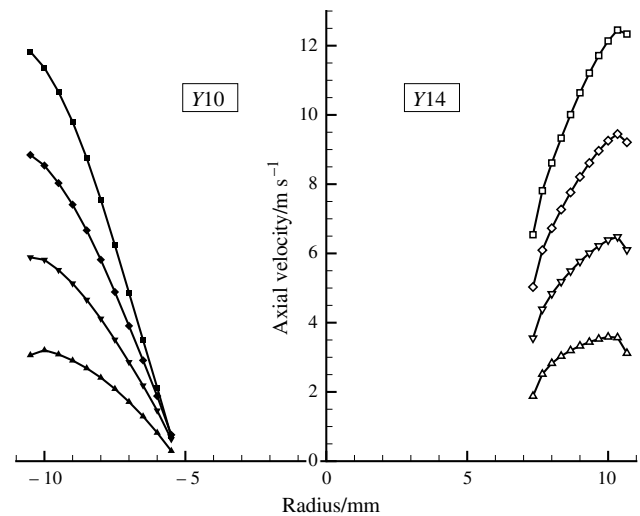

Fig. 15 Axial component of velocity exiting from burner nozzle in non-reacting case for $Y10$ (left) and $Y14$ (right) bluff bodies with air flow rates of 2.5, 4.5, 6.5, and 8.5 m³ h⁻¹

the same, there are some differences. This contour reveals again the very-low-velocity region near the head of the bluff body for $Y10$. The flame tendency to chamber walls in $Y14$ configuration observed before can be seen in the path lines too.

Low flow velocity near the axis facilitates upstream movement of the flame, remembering that combustion worsens the situation by inducing a negative axial velocity due to vortex breakdown. At lower excess air ratios, gas expansion across the flame and the negative induced velocity will be more substantial on one hand and flame speed
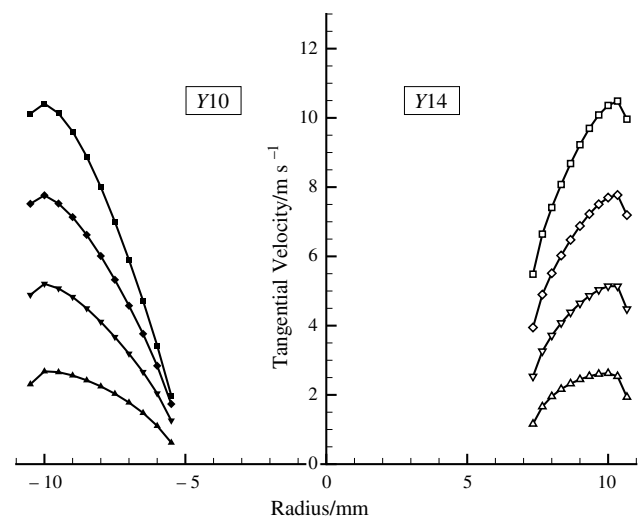

Fig. 16 Tangential component of velocity exiting from burner nozzle in non-reacting case for $Y10$ (left) and $Y14$ (right) bluff bodies with air flow rates of 2.5, 4.5, 6.5, and 8.5 m³ h⁻¹

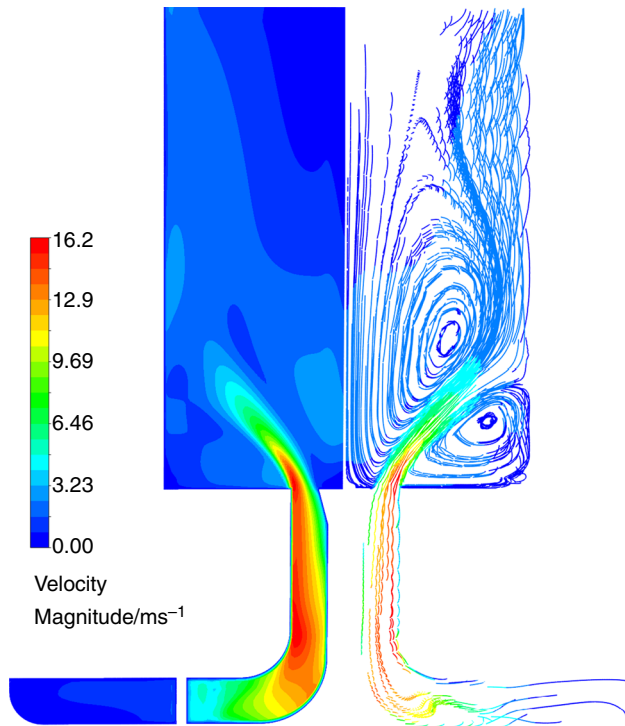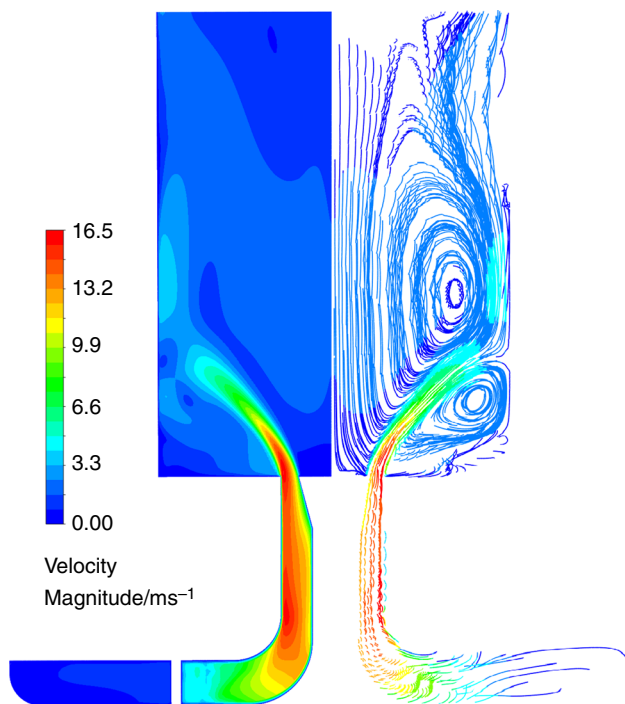**Fig. 17** Velocity magnitude and path lines of $Y10$ and 8.5 m^3 h^{-1} from cold flow simulation
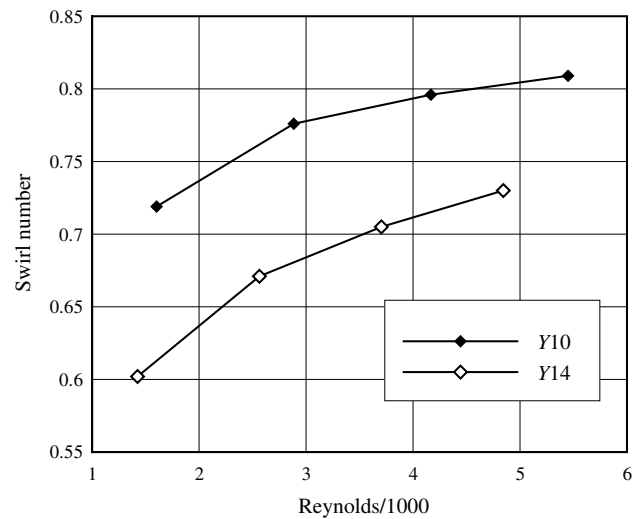

Fig. 19 Flow swirl number of $Y10$ and $Y14$ configurations for different Reynolds numbers

is higher on the other hand. Therefore, it is expected that the burner resistant to flame flashback improves with larger bluff bodies.

Based on these two velocity profiles, the swirl number is calculated and is shown in Fig. 19 for different Reynolds numbers. Here, Reynolds number is calculated based on the average axial velocity and hydraulic diameter of the nozzle annulus. As expected, the swirl number does not depend solely on geometry and increases with Reynolds number. Moreover, the swirl number for $Y14$ configuration, with a thicker bluff body, is always smaller compared to $Y10$ configuration. The difference in the swirl number of these two configurations is approximately 0.1. The swirl number value is close to the value that the burner was designed for. The variation of the swirl number observed here (due to change in either bluff body size or Reynolds number) cannot alter the flame cone angle considerably.

Conclusions

The effect of bluff body size on the stability limits of a swirl burner is investigated. For this purpose, a burner is designed that consumes premixed natural gas and air at room temperature and operated at atmospheric pressure. A radial-type swirler is chosen, and a simple quartz cylindrical combustion chamber surrounds the flame. Various sizes of bluff bodies with a cylindrical shape and an inverted cone at the top are examined. The burner is tested with Reynolds numbers of 640–5300 (based on nozzle average velocity and hydraulic diameter) and thermal powers of 0.95–5.7 kW. The non-reacting flow is also simulated to identify the differences in

Fig. 18 Velocity magnitude and path lines of $Y14$ and 8.5 m^3 h^{-1} from cold flow simulation

the outflow patterns with different bluff bodies. The following results are obtained in this study:

(1) The effect of bluff body size on flame shape is generally not considerable, especially at low excess air ratios. At higher excess air ratios, the flame draws slightly toward the tube walls with larger bluff bodies.

(2) Increasing the diameter of the bluff body causes the flashback limit to shift toward lower excess air ratios, making the flame more resistant against flashback. Changing the ratio of bluff body to nozzle diameter from 0.45 to 0.55 restricts flashback to very low thermal powers only, and if this ratio reaches 0.64, flashback is completely suppressed.

(3) Blowout limit extends to higher excess air ratios with larger bluff bodies at lower thermal powers. This positive effect gradually disappears when the thermal power is increased. Enlarging the ratio of bluff body to nozzle diameter over 0.55 has no effect on blowout.

(4) The cause of improvement of resistance against flashback with larger bluff bodies is the greater axial velocity in the central region of the nozzle. With thinner bluff bodies, the axial velocity near the bluff body is small and combustion-induced vortex breakdown can make it even more smaller, facilitating flame upstream propagation. The swirl number is between 0.6 to 0.8 for different bluff bodies and test conditions.

(5) The corner recirculation zone periodically extinguishes and reignites at excess air ratios near blowout, manifesting itself in high-amplitude low-frequency fluctuations in flame chemiluminescence intensity. This serves as a caution that further increase in air flow will result in blowout. On the contrary, no warning signs are observed before flashback in flame chemiluminescence.

References

1. Dunn-Rankin D. Lean combustion: technology and control. London: Academic Press; 2007.
2. Saboohi Z, Ommi F, Akbari MJ. Multi-objective optimization approach toward conceptual design of gas turbine combustor. Appl Therm Eng. 2019;148:1210–23.
3. Singh OK. Combustion simulation and emission control in natural gas fuelled combustor of gas turbine. J Therm Anal Calorim. 2016;125:949–57.
4. Khatamnejad H, Khalilarya S, Jafarmadar S, Mirsalim M, Gharehghani A, Niaki SOD. Experimental investigation on the effect of natural gas premixed ratio on combustion and emissions in an IDI engine. J Therm Anal Calorim. 2019;138:3977–86.
5. Benim AC, Syed KJ. Flashback mechanisms in lean premixed gas turbine combustion. Oxford: Academic Press; 2014.
6. Hoferichter V, Sattelmayer T. Boundary layer flashback in premixed hydrogen-air flames with acoustic excitation. J Eng Gas Turb Power. 2018;140(5):051502.
7. Baumgartner GM. Flame flashback in premixed hydrogen-air combustion systems. Munich: Technical University of Munich; 2014.
8. Sayad P, Schonborn A, Li M, Klingmann J. Visualization of different flashback mechanisms for H_2/CH_4 mixtures in a variable-swirl burner. J Eng Gas Turb Power. 2015;137(3):031507.
9. Nauert A, Petersson P, Linne M, Dreizler A. Experimental analysis of flashback in lean premixed swirling flames: conditions close to flashback. Exp Fluids. 2007;43:89–100.
10. Heeger C, Gordon RL, Tummers MJ, Sattelmayer T, Dreizler A. Experimental analysis of flashback in lean premixed swirling flames: upstream flame propagation. Exp Fluids. 2010;49:853–63.
11. Fritz J, Kroner M, Sattelmayer T. Flashback in a swirl burner with cylindrical premixing zone. J Eng Gas Turb Power. 2004;126(2):276–83.
12. Ahmed MMA, Birouk M. Effect of fuel nozzle geometry and airflow swirl on the coherent structures of partially premixed methane flame under flashback conditions. Exp Therm Fluid Sci. 2018;99:304–14.
13. Ebi D, Clemens NT. Experimental investigation of upstream flame propagation during boundary layer flashback of swirl flames. Combust Flame. 2016;168:39–52.
14. Reichel TG, Terhaar S, Paschereit O. Increasing flashback resistance in lean premixed swirl-stabilized hydrogen combustion by axial air injection. J Eng Gas Turb Power. 2015;137(7):071503.
15. Tanimura S, Komiyama M, Takeishi K, Iisaki Y. Visualization of flashback in a premixed burner with swirling flow. Sci China Technol Sc. 2010;53(1):40–5.
16. Karimi N, McGrath S, Brown P, Weinkauff J, Dreizler A. Generation of adverse pressure gradient in the circumferential flashback of a premixed flame. Flow Turbul Comb. 2016;97:663–87.
17. Karimi N, Heeger C, Christodoulou L, Dreizler A. Experimental and theoretical investigation of the flashback of a swirling, bluff-body stabilized, premixed flame. Z Phys Chem. 2015;229(5):663–80.
18. Yegian DT, Cheng RK. Development of a lean premixed low-swirl burner for low NOx practical applications. Combust Sci Technol. 1998;139:207–27.
19. Syred N, Giles A, Lewis J, Abdulsada M, Valera Medina A, Marsh R, et al. Effect of inlet and outlet configurations on blow-off and flashback with premixed combustion for methane and a high hydrogen content fuel in a generic swirl burner. Appl Energ. 2014;116:288–96.
20. Konle M, Sattelmayer T. Time scale model for the prediction of the onset of flame flashback driven by combustion induced vortex breakdown. J Eng Gas Turb Power. 2010;132(4):041503.
21. Kroner M, Sattelmayer T, Fritz J, Kiesewetter F, Hirsch C. Flame propagation in swirling flows—effect of Local Extinction on the combustion induced vortex breakdown. Combust Sci Technol. 2007;179:1385–416.
22. Gadiraju S. Study of lean blowout limits and effects of near blowout oscillations on flow field and heat transfer on gas turbine combustor. Blacksburg: Virginia Polytechnic Institute and State University; 2017.
23. Runyon J, Marsha R, Bowen P, Pugh D, Giles A, Morris S. Lean methane flame stability in a premixed generic swirl burner: isothermal flow and atmospheric combustion characterization. Exp Therm Fluid Sci. 2018;92:125–40.
24. Afridi MI, Qasim M, Wakif A, Hussanan A. Second law analysis of dissipative nanofluid flow over a curved surface in the presence of lorentz force: utilization of the Chebyshev–Gauss–Lobatto spectral method. Nanomaterials. 2019;9(195):1–21.

25. Wakif A, Chamkha A, Thumma T, Animasaun IL, Sehaqui R. Thermal radiation and surface roughness effects on the thermo-magneto-hydrodynamic stability of alumina–copper oxide hybrid nanofluids utilizing the generalized Buongiorno's nanofluid model. J Therm Anal Calorim. 2020. https://doi.org/10.1007/s10973-020-09488-z.

26. Wakif A, Boulahia Z, Amine A, Animasaun IL, Afridi MI, Qasim M, et al. Magneto-convection of alumina-water nanofluid within thin horizontal layers using the revised generalized buongiorno's model. Front Heat Mass Transf. 2019;12(3):1–15.

27. Burmberger S, Hirch C, Sattelmayer T. Design rules for the velocity field of vortex breakdown swirl burners. In: Proceedings of ASME Turbo Expo, Barcelona, Spain. 2006;paper no. GT2006-90495:413–21.

28. Jerzak W, Kuznia M. Experimental study of impact of swirl number as well as oxygen and carbon dioxide content in natural gas combustion air on flame flashback and blow-off. J Nat Gas Sci Eng. 2016;29:46–54.

29. Vigueras-Zúñiga MO, Syred N, Valera-Medina A, De la Rosa-Urbalejo D. Flashback avoidance in swirling flow burners. Ingeniería Investigación y Tecnología. 2014;15(4):603–14.

30. Burmberger S, Hirch C, Sattelmayer T. Designing of a radial swirler vortex breakdown burner. In: Proceedings of ASME Turbo Expo, Barcelona, Spain. 2006; paper no. GT2006-90497:423–31.

31. Hatem FA, Alsaegh AS, Al-Faham M, Valera-Medina A, Chong CT, Hassoni SM. Enhancing flame flashback resistance against combustion induced vortex breakdown and boundary layer flashback in swirl burners. Appl Energ. 2018;230:946–59.

32. Wakif A, Boulahia Z, Sehaqui R. Numerical analysis of the onset of longitudinal convective rolls in a porous medium saturated by an electrically conducting nanofluid in the presence of an external magnetic field. Res Phys. 2017;7:2134–52.

33. Chen R, Driscoll JF, Kelly J, Namazian M, Schefer RW. A comparison of bluff-body and swirl-stabilized flames. Combust Sci Technol. 1990;71:197–217.

34. Gentemann A, Hirsch C, Kunze K, Kiesewetter F, Sattelmayer T, Polifke W. Validation of flame transfer function reconstruction for perfectly premixed swirl flames. In: Proceedings of ASME Turbo Expo, Vienna, Austria. 2004; paper no. GT2004-53776:501–10.

35. Palies P, Durox D, Schuller T, Candel S. The combined dynamics of swirler and turbulent premixed swirling flames. Combust Flame. 2010;157:1698–717.

36. Durox D, Moeck JP, Bourgouin JF, Morenton P, Viallon M, Schuller T, Candel S. Flame dynamics of a variable swirl number system and instability control. Combust Flame. 2013;160:1729–42.

37. Tong Y, Liu X, Wang Z, Richter M, Klingmann J. Experimental and numerical study on bluff-body and swirl stabilized diffusion flames. Fuel. 2018;217:352–64.

38. Saediamiri M, Birouk M, Kozinski JA. Flame stability limits of low swirl burner—effect of fuel composition and burner geometry. Fuel. 2017;208:410–22.

39. Sheen HJ, Chen WJ, Jeng SY, Huang TL. Correlation of swirl number for a radial-type swirl generator. Exp Therm Fluid Sci. 1996;12:444–51.

40. Higgins B, McQuay MQ, Lacas F, Rolon JC, Darabiha N, Candel S. Systematic measurements of OH chemiluminescence for fuel-lean, high-pressure, premixed, laminar flames. Fuel. 2001;80:67–74.

41. Higgins B, McQuay MQ, Lacas F, Candel S. An experimental study on the effect of pressure and strain rate on CH chemiluminescence of premixed fuel-lean methane/air flames. Fuel. 2001;80:1583–91.

42. Behzadi M, Ahmadi MH, Ommi F. Hot-film/hot-wire anemometer calibration for low velocities using image processing. Sci Iran. 2019. https://doi.org/10.24200/sci.2019.51318.2119.

43. Wilcox DC. Turbulence modeling for CFD. 3rd ed. Los Angeles: DCW Industries; 2006.

44. Launder BE, Reece GJ, Rodi W. Progress in the development of a Reynolds-stress turbulence closure. J Fluid Mech. 1975;68(3):537–66.

45. Docquier N, Belhalfaoui S, Lacas F, Darabiha N, Rolon C. Experimental and numerical study of chemiluminescence in methane/air high-pressure flames for active control applications. P Combust Inst. 2000;28:1765–74.

46. Lauer M, Sattelmayer T. On the adequacy of chemiluminescence as a measure for heat release in turbulent flames with mixture gradients. J Eng Gas Turb Power. 2010;132(6):061502.

47. Dasch CJ. One-dimensional tomography: a comparison of Abel, onion-peeling, and filtered back projection methods. Appl Opt. 1992;31(8):1146–52.

48. Andrews GE, Bradley D. The burning velocity of methane–air mixtures. Combust Flame. 1972;19:275–88.

49. Khalil A, Brooks JM, Gupta AK. Impact of confinement on flow-field of swirl flow burners. Fuel. 2016;184:1–9.

50. Kabiraj L, Saurabh A, Karimi N, Sailor A, Mastorakos E, Dowling AP, Paschereit CO. Chaos in an imperfectly premixed model combustor. Chaos. 2015;25(2):023101.

51. Pourhoseini SH, Asadi R. An experimental study on thermal and radiative characteristics of natural gas flame in different equivalence ratios by chemiluminescence and IR photography methods. J Nat Gas Sci Eng. 2017;40:126–31.

52. Christodoulou L, Kabiraj L, Saurabh A, Karimi N. Characterizing precursor signature of flame flashback through recurrence analysis. Chaos. 2016;26(1):013110.

53. Schneider C, Dreizler A, Janicka J. Fluid dynamical analysis of atmospheric reacting and isothermal swirling flows. Flow Turbul Combust. 2005;74:103–27.